Static and dynamic magnetism of the Ir-based double perovskites La_2BIrO_6 (B = Co, Zn) probed by magnetic resonance spectroscopies

M. Iakovleva,[1,2,3] S. Fuchs,[1,2] A. Alfonsov,[1] H.-J. Grafe,[1] M. Vogl,[1,2] S. Aswartham,[1] S. Wurmehl,[1] T. Dey,[1] B. Büchner,[1,2] E. Vavilova,[3] and V. Kataev[1]

[1]*Leibniz Institute for Solid State and Materials Research IFW Dresden, 01171 Dresden, Germany*

[2]*Institut für Festkörper- und Materialphysik, Technische Universität Dresden, 01062 Dresden, Germany*

[3]*Zavoisky Physical-Technical Institute of the Russian Academy of Sciences, 420029 Kazan, Russia*

(Received 22 June 2018; published 1 November 2018)

We report the ^{139}La nuclear magnetic resonance (NMR), electron spin resonance (ESR), and complementary magnetometry results on the Ir-based double perovskite compounds La_2BIrO_6 with strongly magnetic Co^{2+} ($3d^7$, $S = 3/2$) and nonmagnetic Zn^{2+} ($3d^{10}$, $S = 0$) ions at the B site. ESR signals from Ir^{4+} ions in La_2ZnIrO_6 and a collective ESR mode of coupled Co^{2+} spins $S = 3/2$ and Ir^{4+} pseudospins $j_{\rm eff} = 1/2$ were observed and studied as a function of temperature and excitation frequency. These signals gradually evolve into a resonance mode of the uncompensated ferromagnetic moments in the antiferromagnetically (AFM) ordered state below $T_N \approx 11$ K and 98 K for La_2ZnIrO_6 and La_2CoIrO_6, respectively. The temperature evolution of the ^{139}La NMR spectra and the nuclear spin relaxation $T_1^{-1}(T)$ reveal three distinct regimes for La_2BIrO_6 (B = Co, Zn): (i) a paramagnetic state at high temperatures; (ii) a short-range AFM order in an extended temperature region above T_N where the ESR modes first appear; (iii) magnetic long-range order at lower T. The extended short-range-ordered regime at temperatures much higher than T_N constitutes evidence of substantial magnetic frustration which appears to be a salient feature of both studied materials.

DOI: 10.1103/PhysRevB.98.174401

I. INTRODUCTION

An intimate interplay of different degrees of freedom—spin, orbital, charge, and lattice—is the remarkable fingerprint of complex 5d iridium oxides which keeps them in the focus of unceasing interdisciplinary attention for already quite some time (for reviews see, e.g., Refs. [1–5]). Their Mott-insulating 3d counterparts exhibit a clear hierarchy of the energy scales with the on-site Coulomb repulsion energy of up to 10 eV being the largest one, as compared with much smaller bandwidths and practically negligible relativistic spin-orbit coupling (SOC) energy. In contrast, these scales in the iridates become roughly similar, equalizing at the level ~0.5 eV. This is because a substantial spatial extension of the 5d orbitals reduces the Mott–Hubbard electron-electron correlation effects and increases the bandwidth, whereas SOC, which scales with the atomic number as Z^2 for the outer electrons [5,6] boosts significantly. In this exotic situation, novel phenomena are expected to occur in complex iridium oxides, such as spin-orbit assisted Mott insulating states with exotic spin orders, quantum spin liquid phases, Weyl semimetallic behavior, and superconductivity (see, e.g. Refs. [2–4]).

One important case of iridates is found in materials adopting the double perovskite structure La_2BIrO_6 with either magnetic (Mn, Fe, Co, Ni, Cu) or nonmagnetic (Mg, Zn) B^{2+} cations. Their crystal structure can be understood as a superposition of the interpenetrating simple perovskite lattices $LaBO_3$ and $LaIrO_3$ with alternating $B^{2+}O_6$ and $Ir^{4+}O_6$ octahedra (Fig. 1). The Ir^{4+} ions are characterized by the effective pseudospin $j_{\rm eff} = 1/2$ ground-state magnetic doublet with a very anisotropic distribution of the spin density. Depending on the lattice geometry, it may provide a realization of different spin models, ranging from the Heisenberg to the Kitaev quantum compass models and their extrapolations which may also incorporate symmetric (pseudodipolar) and antisymmetric (Dzyaloshinskii–Moriya) contributions [7]. In the double perovskite structure multiple intra- and intersublattice exchange pathways are possible where long-range interactions may play an important role [8–10]. As a result, different magnetically ordered ground states were found in these materials. In the case of nonmagnetic B = Mg and Zn, A-type antiferromagnetic (AFM) order was observed below $T_N = 12$ and 7.5 K, respectively [11,12]. The spin structure is collinear in La_2MgIrO_6, whereas the Ir moments are canted in La_2ZnIrO_6. The canting can be understood via a simple model that includes both the Heisenberg exchange and the Dzyaloshinskii–Moriya interaction [11,13]. However, a more intriguing scenario with the dominant Kitaev term has been proposed recently [12]. In the case of magnetic B sites, a complex interplay of the 3d and 5d magnetic sublattices was observed. For example, La_2MnIrO_6 undergoes a ferromagnetic (FM) transition at $T_c = 130$ K [14], whereas La_2FeIrO_6 and La_2NiIrO_6 exhibit both AFM and FM components and the possible ground state is a helical or canted spin structure [15,16]. La_2CuIrO_6 orders below 74 K with a spin structure composed of two orthogonal AFM sublattices characterized by a very small canted moment [17]. In La_2CoIrO_6, Ir^{4+} pseudospins couple AFM to the weak FM moment of the canted Co^{2+} sublattice which is an ordered zigzag AFM (E type) at a temperature slightly below 100 K [18,19]. A crossover from the Co-dominated to the Ir-dominated AFM

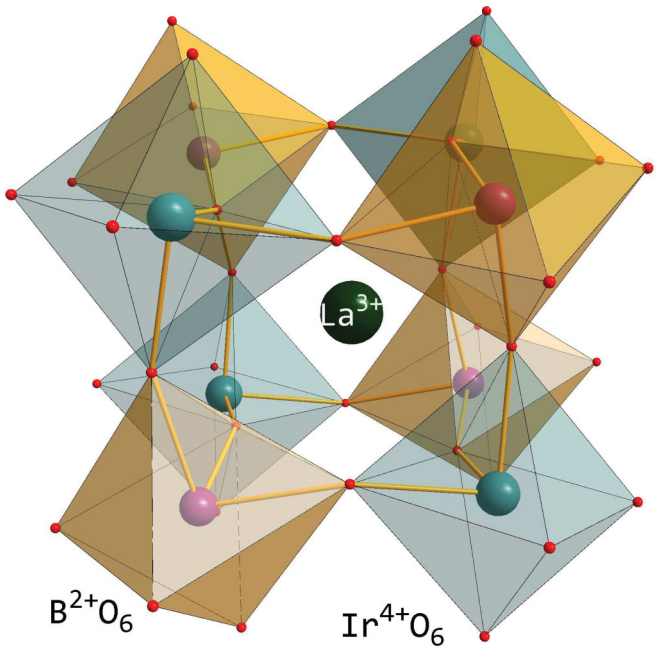

FIG. 1. Crystal structure of La_2BIrO_6 ($B = Co^{2+}$, Zn^{2+}, ...). The La^{3+} ion is located in the center of the cube made out of $B^{2+}O_6$ (light orange) and $Ir^{4+}O_6$ (light blue) metal-oxygen octahedra.

behavior in the substitution series $La_2Zn_{1-x}Ir_xO_6$ was studied in Ref. [20], revealing a reduced magnetic entropy that points towards a large SOC and orbital contribution in the system.

The majority of the studies of this family of iridium-based double perovskites was performed with static magnetic, thermodynamic, and in part with neutron scattering techniques. Magnetic resonance techniques have received much less attention although they could provide valuable insights into the spin dynamics and ordering phenomena on the local scale. Indeed, in our previous work in Ref. [17], a combined electron spin resonance (ESR) and nuclear magnetic resonance (NMR) study of La_2CuIrO_6 revealed a temperature-driven continuous evolution of the low-frequency dynamics of the Cu and Ir spin subsystems which feature short-range correlations slightly above the ordering temperature of 74 K and a gradual crossover with decreasing temperature from the incoherent to coherent joint precession of the interacting sublattices, which finally get locked at the characteristic temperature of 54 K. In this material both sublattices are built of spins (pseudospins) of the same value of $S = 1/2$ (Cu^{2+}, $3d^9$) and $j_{\rm eff} = 1/2$ (Ir^{4+}, $5d^5$).

The goal of the present work is to examine with ESR and NMR spectroscopies the coexistence of the Ir^{4+} pseudospin $j_{\rm eff} = 1/2$ sublattice with either the strongly magnetic ($B = Co^{2+}$, $3d^7$, $S = 3/2$) sublattice or the nonmagnetic ($B = Zn$, $3d^{10}$, $S = 0$) sublattice realized in La_2CoIrO_6 and La_2ZnIrO_6 compounds, respectively, and to evaluate the respective roles of the $3d$ and $5d$ spin subsystems for the static and dynamic magnetism of La_2BIrO_6, considering also the previous results on La_2CuIrO_6. Indeed, our ESR and ^{139}La NMR data demonstrate an interesting evolution of the electron spin dynamics in both compounds over the entire temperature range of study. In particular, we find an extended temperature region of the short-range spin order which intervenes between the paramagnetic state at high temperatures and the long-range ordered state below T_N. We qualitatively discuss this remarkable observation as a signature of magnetic frustration which we relate to a manifold of factors, such as an inherent geometrical frustration in the double perovskites, and, in particular, multiple long-range exchange pathways yielding competing exchange interactions with strong anisotropy, characteristic of $5d$ double perovskites with strong spin-orbit coupling.

The paper is organized as follows: Sample preparation and details of the used experimental techniques are described in Sec. II. In Secs. III A–III C bulk magnetic measurements data and the results of ESR and NMR experiments, respectively, are presented and analyzed. Section IV is dedicated to the discussion. Finally, major conclusions are summarized in Sec. V.

II. EXPERIMENTAL DETAILS

Polycrystalline samples of La_2ZnIrO_6 and La_2CoIrO_6 were prepared by a conventional solid-state reaction method. Details of their synthesis and primary characterization with x-ray diffraction, scanning electron microscopy (SEM), and energy-dispersive x-ray spectroscopy (EDXS) was reported in Ref. [20]. Both compounds are found to crystallize in the monoclinic space group $P\,2_1/n$ with the very similar cell parameters, as expected due to almost equal ionic radii of the high-spin Co^{2+} and Zn^{2+}. SEM and EDXS confirm the chemical homogeneity and the targeted stoichiometry of the samples.

^{139}La NMR experiments were performed on the powder samples shielded in a quartz tube. The probed ^{139}La nuclei are characterized by spin $I = 7/2$, natural abundance of 99.1%, a quadrupole moment $Q = 0.21$ barns, and a gyromagnetic ratio $\gamma_n = 6.014$ MHz T^{-1}. The data were collected by using a Tecmag pulse solid-state NMR spectrometer with a 0–9.2 T superconducting magnet from Magnex Scientific equipped with a ^{4}He variable-temperature inset. The spectra were recorded by sweeping magnetic field at a constant frequency $\nu_0 = 42.1$ MHz and integrating at each field step the intensity of the spin echo obtained with the conventional Hahn-echo pulse sequence ($\pi/2$-τ-π). For the spin-lattice relaxation rate measurements the stimulated echo sequence ($\pi/2$-τ_1-$\pi/2$-τ_2-$\pi/2$) was employed.

ESR measurements at $\sim$10 GHz were performed with a commercial X-band ESR spectrometer from Bruker. Measurements at higher frequencies were carried out with a homemade high-field multi-frequency ESR spectrometer [21] upgraded with the PNA-X Network Analyzer from Keysight Technologies. In this setup, magnetic fields up to 16 T were obtained with a solenoid superconducting magnet from Oxford Instruments equipped with a ^{4}He variable-temperature insert.

Bulk magnetic measurements were done with a Quantum Design MPMS-XL SQUID magnetometer.

III. RESULTS

A. Bulk magnetic properties

Basic static magnetic properties of the La_2ZnIrO_6 and La_2CoIrO_6 samples studied in the present work were

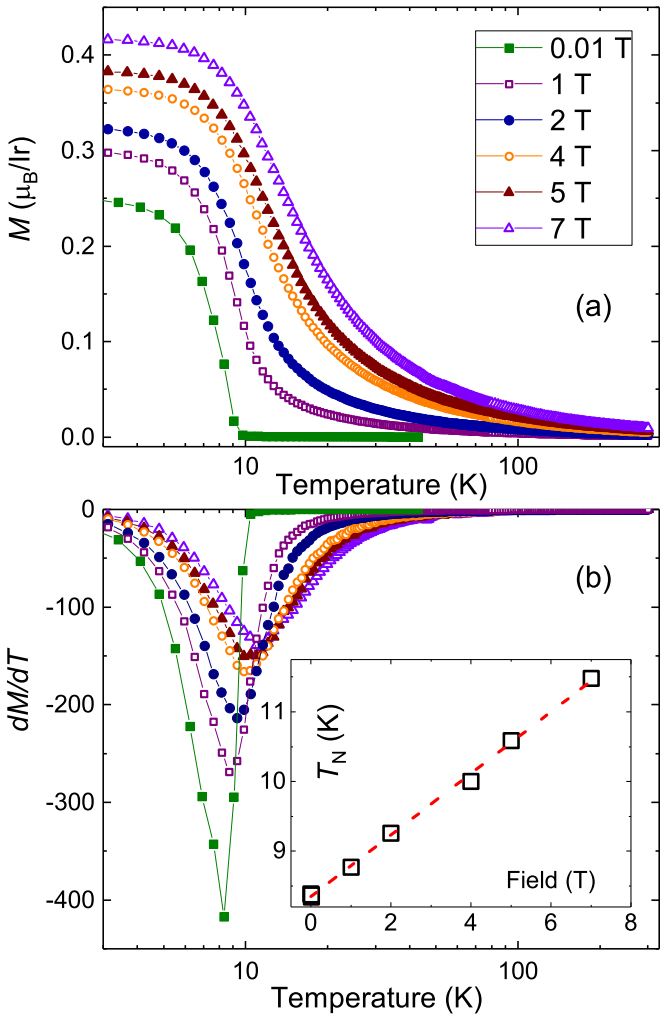

FIG. 2. (a) Temperature dependence of the static magnetization $M(T)$ of La_2ZnIrO_6 measured in the field-cooled mode at several fields in the range 0.01–7 T. (b) Temperature dependence of the derivative $dM(T)/dT$. The inset shows the field dependence of the ordering temperature T_N determined from the peak of $dM(T)/dT$.

investigated in Ref. [20] and agree with the results of other groups [13,18]. Here we report additional measurements necessary for the analysis of the magnetic resonance data, e.g., as a function of field.

The temperature dependence of the static magnetization $M(T)$ of the La_2ZnIrO_6 samples measured at different fields up to 7 T is shown in Fig. 2(a). The ordering temperature T_N was determined from the peak of the derivative $dM(T)/dT$ [Fig. 2(b)]. T_N increases linear with field as shown in the inset of Fig. 2(b). Above ~15 K the static susceptibility $\chi = M/H$ is field independent, implying a linear relation M vs H. At 10 K the $M(H)$ dependence acquires an S-like shape and shows a small hysteresis at lower temperatures (Fig. 3). At stronger fields $M(H)$ increases linearly which is typical for the canted AFM spin structure as determined for La_2ZnIrO_6 in Refs. [11,12].

In addition, we have measured the ac-susceptibility of La_2ZnIrO_6 which did not reveal a frequency dependence, thus

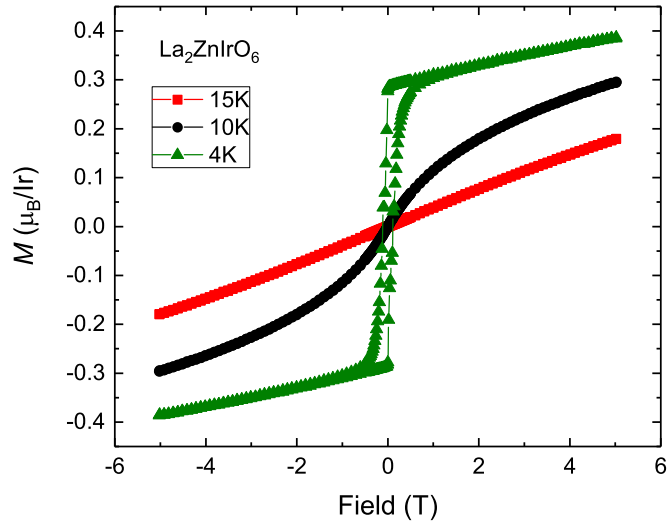

FIG. 3. Field dependence of the static magnetization $M(H)$ of La_2ZnIrO_6 measured at selected temperatures in the range 1.8–15 K.

excluding a spin-glass-like behavior in the whole temperature range (Fig. 4). Interestingly, the peak in the ac susceptibility reveals a double structure which is also visible in the $dM(T)/dT$ peak in small magnetic fields. This structure broadens by increasing the dc-field strength. A similar feature that is suppressed by a magnetic field was observed in the $M(H)$ data in Ref. [13] and in the specific heat data in Ref. [20].

Measurements of the $M(T)$ dependence for the La_2CoIrO_6 sample reveal, similar to La_2ZnIrO_6, an increase of T_N with increasing field strength, as shown in Fig. 5.

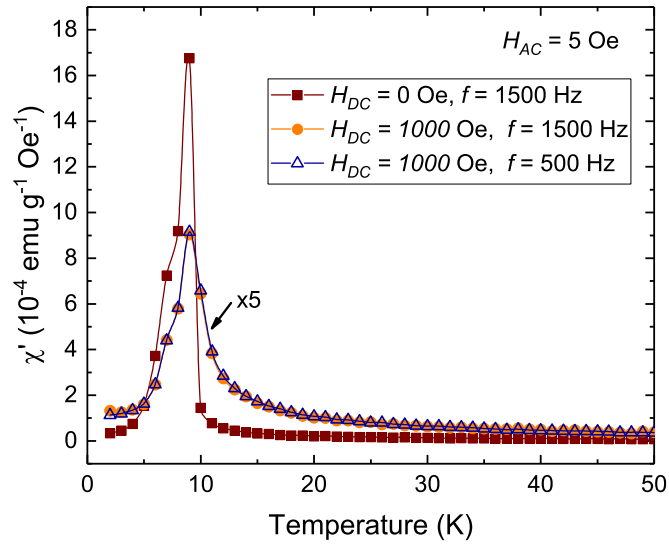

FIG. 4. Temperature dependence of the ac susceptibility $\chi'(T)$ measured at frequencies of 500 Hz (triangles) and 1500 Hz (circles) in a static field of 1000 Oe. Note that the curves are practically indistinguishable. The $\chi'(T)$ dependence at 1500 Hz in zero static field is plotted by squares. In all measurements the strength of the ac field amounts to 5 Oe.

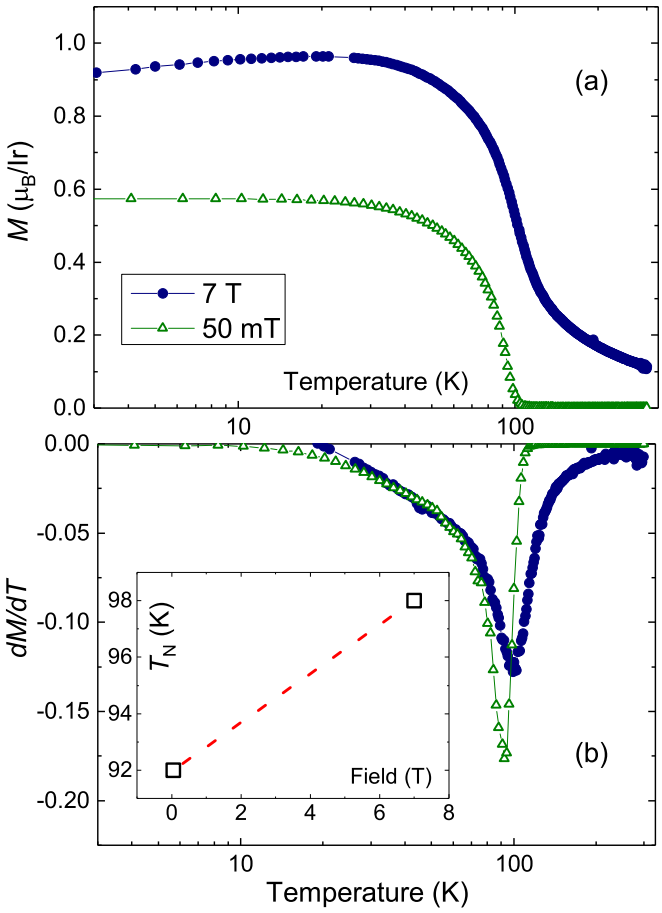

FIG. 5. (a) Temperature dependence of the static magnetization $M(T)$ of La_2CoIrO_6 measured in the field-cooled mode at 0.05 and 7 T. (b) Temperature dependence of the derivative $dM(T)/dT$. The inset shows the field dependence of the ordering temperature T_N determined from the peak of $dM(T)/dT$.

B. Electron-spin resonance spectroscopy

1. La_2ZnIrO_6

ESR response from a powder sample of La_2ZnIrO_6 could be detected at temperatures below ~30 K. Two type of signals can be observed in the spectrum: an asymmetric signal at a field corresponding to the g factor of order two (Fig. 6, inset), and a broad feature emerging practically at zero magnetic field (Fig. 7). The former signal has a typical powder pattern arising due to the averaging of the anisotropic g factor with the left-side peak corresponding to $g_\perp$ and the right-side shoulder corresponding to the $g_\parallel$ components of the g tensor, respectively [22]. From ESR measurements at several selected excitation frequencies ν and different temperatures a relationship between ν and the field position of the peak and the shoulder H_{res} can be obtained, as exemplified in Fig. 6. At each temperature this relationship can be well fit with the linear dependence

$$h\nu = g\mu_0\mu_B H_{res} + \Delta, \qquad (1)$$

where Δ is the zero-field magnetic anisotropy gap, and h, μ_B, and μ_0 are the Planck constant, Bohr magneton, and vacuum permeability, respectively. The fits yield $g_\parallel = 1.69$ and $g_\perp = 2.03$ independent of temperature, within the experimental

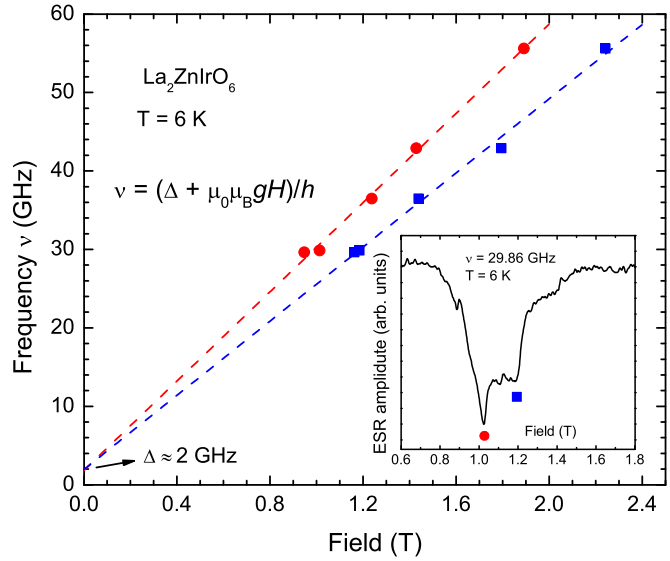

FIG. 6. Relationship between the frequency ν and the field $\mu_0 H_{res}$ corresponding to the peak (circles) and the shoulder (squares) of the asymmetric ESR powder signal of La_2ZnIrO_6 (inset) at $T = 6$ K. Solid lines are fits to Eq. (1).

accuracy, in the whole studied range 4–20 K. Δ is practically zero at higher temperatures whereas it acquires a small but finite value $\Delta \approx 2$ GHz upon entering the magnetically ordered state of La_2ZnIrO_6 below $T_N \approx 11$ K.

The anisotropy of the g factor with $g_\perp > 2 > g_\parallel$ is generally expected for the Ir^{4+} ion in the case of the elongation of the surrounding octahedron of oxygen ligands [23], although some exceptions are possible [24]. Indeed, in La_2ZnIrO_6 the Ir–O bonds in the equatorial plane of the IrO_6 octa-

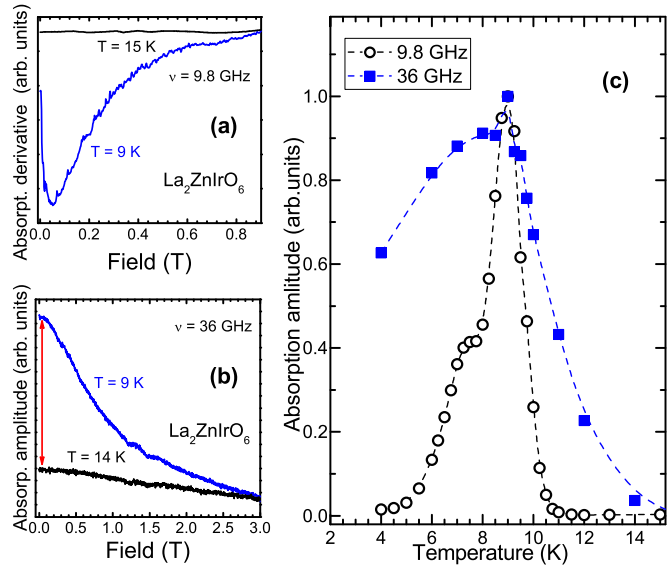

FIG. 7. Low-field part of the ESR spectra of La_2ZnIrO_6 at (a) $\nu = 9.8$ GHz and (b) 36 GHz. Note that, in panel (a), the signal is the field derivative of the absorption recorded with the X-band spectrometer. Panel (c) depicts the amplitude of the low-field microwave absorbtion as a function of temperature.

hedron amount pairwise to 1.961 Å and 1.946 Å, whereas the bonds along the elongation axis are appreciably longer (1.991 Å) [25]. This enables to assign the observed ESR signal to the response of the Ir^{4+} ions. The signal does not experience strong changes in the ordered state besides opening a small gap of ∼2 GHz. According to the inelastic neutron scattering study of La_2ZnIrO_6 in Ref. [12], the energy gap for the spin-wave excitations of the Ir AFM sublattices amounts to ∼2 meV (≈500 GHz). Thus the resonance response at a much smaller excitation frequency close to its paramagnetic value and characterized by a zero-field magnetic anisotropy gap much smaller than the AFM spin-wave gap can be attributed to the low-frequency ferromagnetic-like mode of the net sublattice moments arising in the noncollinear AFM spin structures [26–28].

The other feature of the ESR spectrum, namely, the low-field signal (Fig. 7), emerges in the vicinity of T_N. The absorption starts always at zero field, independent of frequency, suggesting its nonresonant nature [Figs. 7(a) and 7(b)]. At the smallest studied frequency of 9.8 GHz the signal raises sharp at T_N and rapidly decreases again revealing a shoulder at ∼8 K in the dependence of its amplitude on temperature $A_{mwa}(T)$ [Fig. 7(c)]. At higher frequencies $A_{mwa}(T)$ is also peaked at T_N though covering a broader temperature range as compared with the 9.8 GHz data [Fig. 7(c)].

The zero-field absorption is known to be related to interaction of microwaves with magnetic domains in a ferromagnet with random directions of the magnetization of local domains at small fields, often referred to as multidomain ferromagnetic resonance [29]. It always starts at zero field, independent of frequency ν, and may have a complicated dependence of intensity on ν (see, e.g. Refs. [30]). Although La_2ZnIrO_6 is an antiferromagnet, an occurrence of weak ferromagnetic moments may presumably cause the formation of ferromagnetic-like domains in the sample, thus explaining this peculiar observation. The shoulder in the peak, which is also present in the ac-susceptibility curve (cf. Figs. 7 and 4), might be related to some reorganization of the domain structure. Interestingly, at higher frequencies the zero-field absorption sets in already above T_N, suggesting that, on the short picosecond timescale, such domains could be preformed even before the static magnetic order has been fully developed.

We note that these two types of signals (Figs. 6 and 7) were previously reported in Ref. [13]. However, since the measurements were performed there only at a single frequency of 9.4 GHz and no frequency dependence was studied, the zero-field signal and the signal at a field corresponding to $g \sim 2$ were, in contradiction to the above analysis, incorrectly assigned to a ferromagnetic resonance and to an AFM resonance, respectively.

2. La_2CoIrO_6

The ESR response of a polycrystalline sample of La_2CoIrO_6 is characterized by a single line which shape in as-measured spectra appears as a mixture of the Lorentzian absorption an dispersion due to the complex impedance of the broadband waveguide of the ESR setup [Fig. 8(e)]. However, since the ESR setup is controlled by the vector network analyzer which measures both the amplitude and the phase

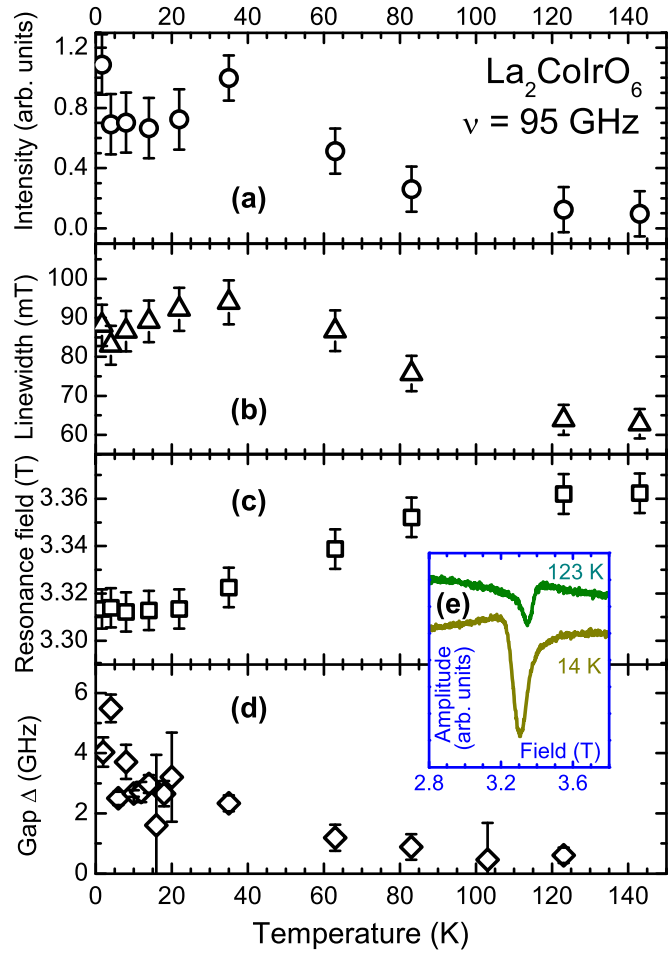

FIG. 8. Temperature dependence of the (a) intensity, (b) linewidth, and (c) resonance field of the ESR signal of La_2CoIrO_6 at $\nu = 95$ GHz, and (d) of the excitation gap Δ evaluated according to Eq. (1). Typical spectra at this frequency are shown in panel (e). Small asymmetry of the ESR line appears due to an admixture of the dispersion signal caused by the complex impedance of the broadband waveguides in the high-field ESR setup and can be corrected by the network analyzer's software.

shift of the detected signal, the true Lorentzian lineshape can be recovered by the analyzer's software. The parameters of the signal, the integrated intensity I, the linewidth δH and the resonance field H_{res} are plotted as a function of temperature for a selected frequency $\nu = 95$ GHz in Figs. 8(a)–8(c). In addition to the T-dependent measurements, the ESR signal has been measured at selected fixed temperatures at different excitation frequencies ν. The so-obtained data were fit with Eq. (1). The g factor reveals a continuous decrease from $g \approx 2.02$ at $T = 143$ K to $g \approx 1.96$ at $T = 2$ K. The excitation gap Δ obtained from the same fit is plotted as a function of T in Fig. 8(d).

Similar to the case of La_2CuIrO_6 [17], the Lorentzian-shaped signal occurring at a field corresponding to the g factor close to two suggests that the signal originates from the joint precession of the exchange-coupled subsystems of Co and Ir spins in the short-range-correlated regime above the ordering temperature T_N, which varies between 92 and 98 K depending on the applied field (Fig. 5). Although the

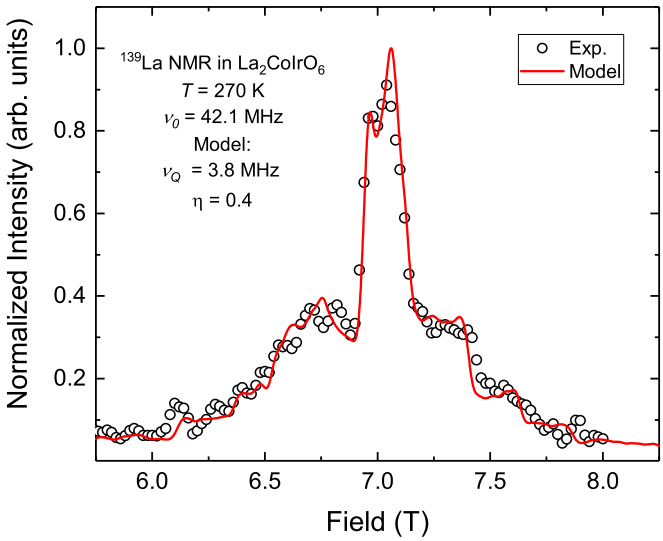

FIG. 9. Experimental ^{139}La NMR field swept spectrum of La_2CoIrO_6 at $T = 270$ K. The red solid line is the result of the modeling according to Eq. (2) (see text).

g tensor of Co^{2+} in a distorted ligand coordination could be strongly anisotropic with $g_z \gg g_x \sim g_y \sim 2$, often most of the spectral weight of the powder-averaged ESR signal is located close to $g \sim 2$. The closeness of the g tensor of Ir^{4+} to the value of two (Sec. III B 1) enables thus the formation of the collective resonance mode above T_N analogous to that in La_2CuIrO_6 [17]. Upon lowering the temperature below T_N this signal gradually transforms into the ferromagnetic-like mode of the precessing uncompensated moments of the AFM sublattices characterized by opening of a small excitation gap of the order $\Delta \sim 4$ GHz at low temperatures [Fig. 8(d)]. This signal is unlikely to be related to the "true" AFM magnon mode of the precessing sublattice magnetization since, similar to La_2ZnIrO_6, it is expected to have a substantially larger gap of the order of some meV [12].

A smooth evolution of the dependencies $I(T)$, $\delta H(T)$, and $H_{res}(T)$ below T_N indicate that the formation of the robustly coupled Co- and Ir-based spin sublattices is not completed at T_N. These dependencies saturate at a much lower temperature of ~30 K which can be considered as a characteristic temperature at which the Ir spin subsystem eventually gets firmly "locked" to a stronger magnetic subsystem of Co spins, qualitatively similar to the dynamics of Ir and Cu spins observed by ESR in La_2CuIrO_6 [17].

C. ^{139}La NMR of La_2ZnIrO_6 and La_2CoIrO_6

For NMR measurements we used ^{139}La as a sensitive probe of the electron spin system. Each La nucleus is located almost in the center of the Co/Zn-Ir cube (Fig. 1) and is surrounded by four Ir magnetic moments and, in the case of La_2CoIrO_6, also by four Co moments, which makes this nucleus sensitive to the uncompensated local fields. ^{139}La has a nuclear spin $I = 7/2$ and therefore possesses an electric quadrupole moment which interacts with the electric field gradient (EFG) from surrounding charges thus giving rise to quadrupole satellites in the spectrum. A typical high-temperature spectrum is shown in Fig. 9. It consists of a narrow central line and broad shoulders due to the quadrupole satellites. The general Hamiltonian describing the NMR spectra reads [31]

$$\mathcal{H} = -\gamma_n \hbar \hat{I}_z H_0 + \hat{I} A_{\alpha\alpha} \hat{S} + \frac{e^2 q Q}{4I(2I-1)}\left[3\hat{I}_{z'}^2 - \hat{I}^2 + \frac{\eta}{2}(\hat{I}_+^2 + \hat{I}_-^2)\right]. \quad (2)$$

Here, γ_n is the gyromagnetic ratio of the nucleus, $\hbar$ is the reduced Planck constant, e is the elementary charge, and Q is the quadrupole moment of the nucleus. The first term in the Hamiltonian describes the Zeeman interaction of the nuclear spin $\hat{I}$ with the external magnetic field H_0. The second term represents the hyperfine interaction of the electron spin $\hat{S}$ with the nuclear system and is determined by the hyperfine tensor $A_{\alpha\alpha}$. The last term stands for the quadrupolar interaction of the nuclear spin with the electric field gradient tensor $V_{\alpha\alpha}$. Here, q and η are the so-called electric field gradient and the asymmetry parameters, defined as $eq = V_{zz}$ and $\eta = \frac{V_{yy}-V_{xx}}{V_{zz}}$. At high temperature, where a contribution of the hyperfine interaction is small due to fast thermal spin fluctuations, the spectrum can be reasonably well modeled by a sum of the first and the last terms of Eq. (2) and the hyperfine interaction is taken implicitly into account via the linewidth parameter. The powder averaging was used in the modeling and the result of calculation is shown in Fig. 9 by the red solid line. From the modeling of the experimental spectrum of La_2CoIrO_6 the quadrupolar frequency $\nu_Q = \frac{3e^2qQ}{2I(2I-1)} = 3.8$ MHz and the EFG tensor asymmetry parameter $\eta = 0.4$ were determined. These values for the La_2ZnIrO_6 compound amount to $\nu_Q = 3.7$ Hz and $\eta = 0.38$. The NMR spectrum features quadrupole satellites and is quite broad already at room temperature, giving evidence for a noncubic symmetry of the local charge surrounding. A quite large value of the asymmetry parameter η is likely to be related to the displacement of oxygens due to the rotation of the metal ion-oxygen octahedra as well as due to a significant spatial extension of the Ir $5d$ orbitals.

1. *Temperature dependence of* ^{139}La *NMR linewidth*

The temperature dependencies of the ^{139}La NMR spectra for both La_2CoIrO_6 and La_2ZnIrO_6 are presented in Figs. 10 and 11, respectively. With decreasing temperature they continuously change for both materials. The width of the spectrum on the half-height is shown for La_2CoIrO_6 in Fig. 12. By lowering the temperature from 300 K down to 120 K the linewidth follows the bulk magnetization measured at a field of 7 T (blue line in Fig. 12). This means that the broadening is of a magnetic nature and is dominated by interactions of the ^{139}La nuclear spins with the Co^{2+} and Ir^{4+} electron subsystems. At $T < 120$ K the spectrum acquires a dome shape and strongly broadens. Finally, at the ordering temperature $T_N = 98$ K at 7 T (Fig. 5) the spectrum broadens even more and acquires an extended, almost flat central part.

Such substantial broadening can be ascribed to the development of a specific distribution of internal fields B_{loc} in the magnetically ordered phase. The low-temperature part of the T dependence (Fig. 12) can be described in the mean-field approximation as $B_{loc} \propto [1 - (T/T_N)^\alpha]^\beta$, where $\alpha \approx 2$, $\beta \approx 0.5$, and $T_N = 98$ K (Fig. 12).

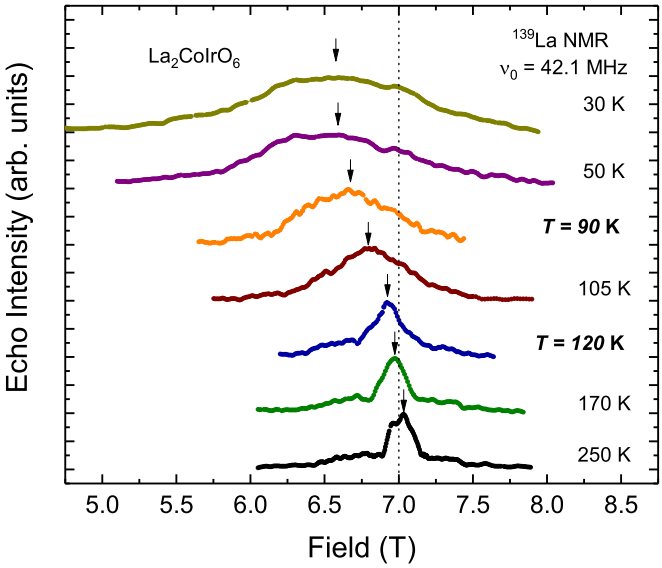

FIG. 10. Temperature evolution of the ^{139}La NMR spectrum of La_2CoIrO_6.

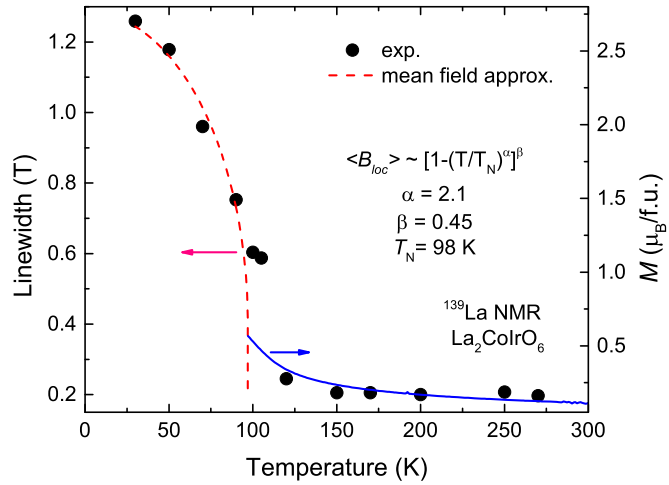

FIG. 12. Temperature dependence of the ^{139}La NMR linewidth for La_2CoIrO_6. The red dashed line denotes the mean-field approximation (see the text for details) with the temperature-independent offset of 0.2 T. The magnetization curve measured at a field of 7 T is shown by the blue solid line.

The ^{139}La NMR linewidth in La_2ZnIrO_6 follows the bulk magnetization $M(T)$ almost in the whole temperature range down to 30 K (Fig. 13). Below this temperature it increases even stronger than M and reaches a plateau at $T \approx 9$ K.

Note that, for both materials, the spectra begin to rapidly broaden and change the shape at temperatures significantly higher than the respective magnetic ordering temperatures, where an additional spectral transformation takes place.

2. *Temperature dependence of ^{139}La NMR line position*

The temperature dependencies of the ^{139}La NMR line shift $K(T)$ are shown in Figs. 14 and 15 for La_2CoIrO_6 and La_2ZnIrO_6, respectively. They were obtained from the position of the center of gravity of the NMR spectra depicted by arrows in Figs. 10 and 11. At high temperatures, its position coincides with the result of the modeling with Eq. (2).

In general, the NMR line shift can be written as $K = K(T) + K_{\rm orb}$, where the second term $K_{\rm orb}$ is due to an orbital contribution, which is T independent. Additionally, the central transition is affected by the second order electric quadrupole interaction. In general, it depends on temperature but here this contribution is assumed to be constant because no significant changes in the lattice parameters are found [18] and thus a temperature variation of ν_Q due to the electron-phonon coupling should be much smaller than the observed magnetic shift. Also, a possible T dependence due to the lattice effects might be compensated by an opposite T dependence of the local charge distribution. The quadrupolar part of the shift is subtracted from the data shown. The temperature dependent

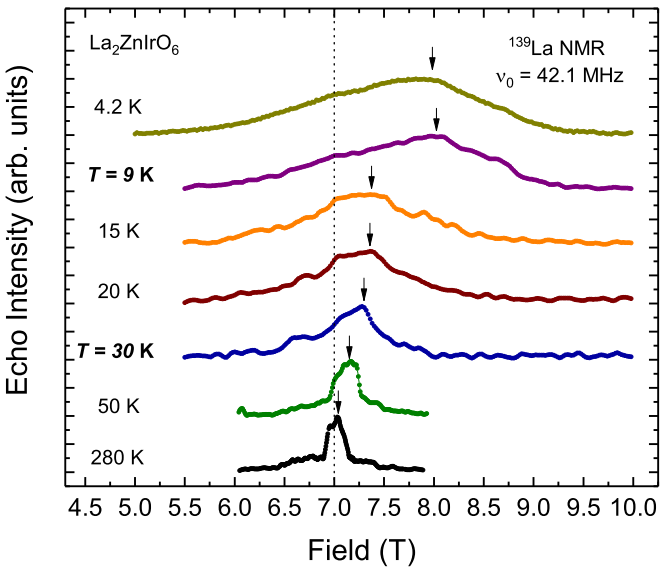

FIG. 11. Temperature evolution of the ^{139}La NMR spectrum of La_2ZnIrO_6.

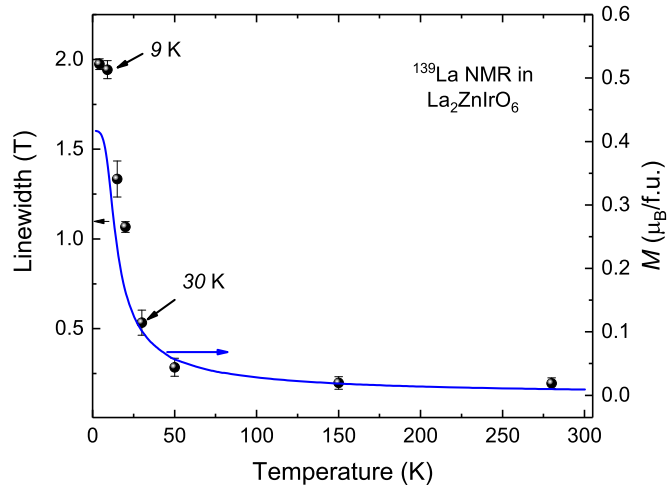

FIG. 13. Temperature dependence of the ^{139}La NMR linewidth for La_2ZnIrO_6. The blue solid line is the magnetization curve measured at a field of 7 T.

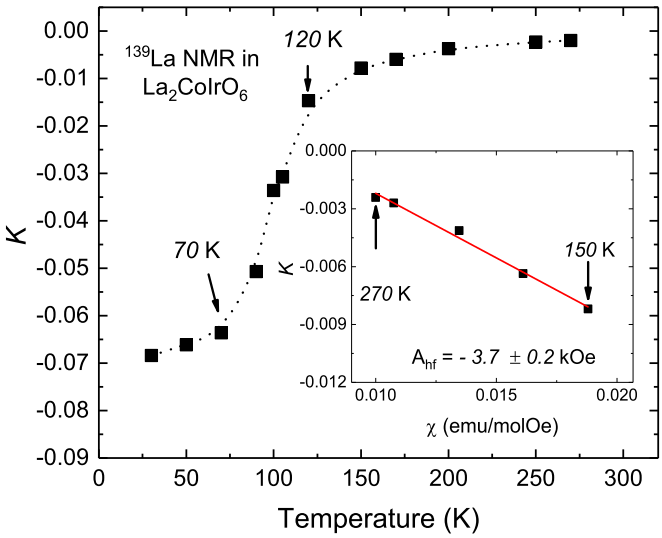

FIG. 14. (main panel) Temperature dependence of the ^{139}La NMR line shift K for La_2CoIrO_6. Dotted line is the guide for the eye. Inset shows K vs χ plot for La_2CoIrO_6. Red solid line is the linear fit (see text).

line shift is proportional to the local static magnetic susceptibility, and in the paramagnetic state it is determined by the static uniform susceptibility of the electron spins, which are coupled to the resonating nuclei according to $K(T) = A_{\rm hf}\chi(T)$. Here $A_{\rm hf}$ is the hyperfine coupling constant. From the linear approximation of the high-temperature part of the K vs χ dependence presented in the insets to Figs. 14 and 15, the averaged hyperfine coupling constants were determined: $A_{\rm hf} = 3.8 \pm 0.2\,{\rm kOe}/\mu_B$ for La_2CoIrO_6 and $A_{\rm hf} = -12.1 \pm 0.2\,{\rm kOe}/\mu_B$ for La_2ZnIrO_6. Note that, for La_2CoIrO_6, the linear regime of K vs bulk χ ceases below 120 K, and below the ordering temperature $T_{\rm N} = 98$ K at 7 T the NMR

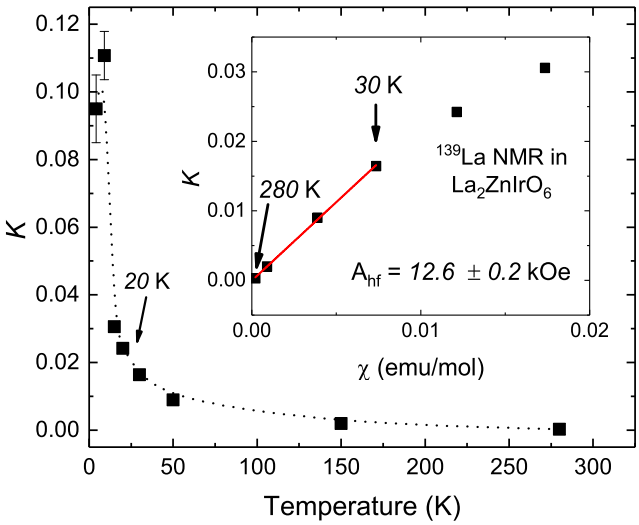

FIG. 15. (main panel) Temperature dependence of the ^{139}La NMR line shift K in La_2ZnIrO_6. Dotted line is the guide for the eye. Inset shows K vs χ plot for La_2ZnIrO_6. Red solid line is the linear fit (see text).

TABLE I. Dipolar hyperfine tensor elements $A_{\alpha\beta}$ of the Hamiltonian (3) calculated selectively for the coupling of ^{139}La nuclei to Co, Cu, and Ir magnetic subsystems (kOe/μ_B).

Compound	A_{xx}	A_{yy}	A_{zz}	A_{xy}	A_{xz}	A_{yz}
La_2CoIrO_6						
Co	−0.51	0.46	0.05	−0.05	−0.26	2.45
Ir	0.40	−0.44	0.04	−0.05	0.27	−2.34
La_2CuIrO_6						
Cu	0.12	−0.43	0.31	3.18	−0.47	0.62
Ir	0.27	−0.42	0.16	−3.21	−0.46	−0.62
La_2ZnIrO_6						
Ir	0.03	−0.12	0.09	−0.08	−0.44	2.57

spectrum changes its shape and does not shift anymore. A similar evolution of the spectrum takes place in La_2ZnIrO_6, although on a different, lower temperature scale. Due to the positive hyperfine coupling for the La_2CoIrO_6 compound with magnetic Co^{2+} ($S = 3/2$) ions the line shifts towards lower fields, whereas for the La_2ZnIrO_6 compound with nonmagnetic Zn ($S = 0$) ions the line shifts to higher magnetic fields due to the negative hyperfine coupling. Note that, in the case of La_2CuIrO_6, with magnetic Cu ($S = 1/2$) ions, the line shift has the same sign as in La_2CoIrO_6 although its magnitude is smaller [17]. The reason for the different signs is that the ^{139}La nuclear spins in La_2ZnIrO_6 couple only to the Ir 5d moments, whereas the nuclear spins in La_2CuIrO_6 and La_2CoIrO_6 also couple to the magnetic 3d electron subsystems of the Cu and Co. Then, the coupling to the Ir 5d moments must be negative, and the coupling to the 3d moments must be positive, and larger than the negative coupling to the Ir 5d moments. There are only two possibilities for a negative hyperfine coupling. The first one is the dipolar hyperfine field of an unpaired electron without spin density at a nuclear site, and the second one is a hyperfine coupling via core polarization. For the dipolar case, we calculated the dipolar hyperfine field of the Cu and Co 3d moments and that of the Ir 5d moments at the ^{139}La nuclear site:

$$\begin{aligned}\hat{H}_{\rm dip} &= -\gamma_n\mu_0\mathbf{I}\cdot\mathbf{H_{dip}}\\ &= -\frac{\mu_0}{4\pi}\gamma_n\gamma_e\sum_j\frac{3(\mathbf{I}\cdot\mathbf{r}_j)(\mathbf{S}_j\cdot\mathbf{r}_j)-\mathbf{S}_j(\mathbf{r}_j\cdot\mathbf{r}_j)}{\mathbf{r}_j^5}\\ &= -\frac{\mu_0}{4\pi}\gamma_n\gamma_e\sum_j\mathbf{I}^T\begin{pmatrix}\frac{3x_j^2-r_j^2}{r_j^5} & \frac{3x_jy_j}{r_j^5} & \frac{3x_jz_j}{r_j^5}\\ \frac{3y_jx_j}{r_j^5} & \frac{3y_j^2-r_j^2}{r_j^5} & \frac{3y_jz_j}{r_j^5}\\ \frac{3z_jx_j}{r_j^5} & \frac{3z_jy_j}{r_j^5} & \frac{3z_j^2-r_j^2}{r_j^5}\end{pmatrix}\mathbf{S}_j\\ &= -\sum_j\mathbf{I}^T A_{j,\rm dip}\mathbf{S}_j. \qquad (3)\end{aligned}$$

Here, $\mathbf{r}_j$ is the radius vector from the position of the nucleus $\mathbf{I}$ to the site of the unpaired electron $\mathbf{S}_j$, and the variables x_j, y_j, and z_j are the vector components of $\mathbf{r}_j$. The corresponding matrix elements of the dipolar hyperfine tensors $A_{\rm j,dip}$ from nearest Co, Cu, and Ir ions are listed in Table I. Apparently, the dipolar hyperfine coupling is an order of magnitude smaller

than the experimentally determined values of A_{hf} (see above), and there are positive and negative values of the diagonal elements for La_2ZnIrO_6 as well as for La_2CoIrO_6. Therefore, we believe that for the negative coupling to the Ir $5d$ moments, only the core polarization can be at play. Since the La ions are *a priori* not carrying the spin density, there must be a transfer of spin density from the Ir ions. Indeed, it has been theoretically suggested that the $4d$ orbitals of the nonmagnetic rare-earth cation play an important role for mediating the exchange interaction between the magnetic $5d^5$ ions in the double perovskites [10]. These unpaired d electrons in the La orbitals then polarize full s shell electrons, where due to the Pauli exclusion principle the antiparallel polarization is preferred, leading to a negative hyperfine coupling. Also, the positive coupling to the Cu or Co $3d$ electrons cannot be dipolar, but must be a transferred hyperfine coupling. Since it is positive, it cannot be due to core polarization. Rather, there might be small admixtures of Cu or Co $3d$ electron and unpaired La s electron wave functions, which have a finite probability density at the ^{139}La nucleus, and thus mediating the Cu or Co $3d$ electron spin density to the ^{139}La nucleus.

3. ^{139}La *spin-lattice relaxation rate*

To probe the dynamic properties of the electron spin system we have used nuclear relaxation measurements. The nuclear spin-lattice relaxation rate T_1^{-1} was measured at the maximum of the ^{139}La NMR line intensity by the stimulated echo sequence. Since the quadrupole splitting of the spectrum is comparable with the widths of the inhomogeneously broadened lines not only the central transition but also the satellite transitions contribute to the detected signal. In this situation the use of the formula

$$M(t) = M_0 e^{-(t/T_1)^b} \tag{4}$$

has enabled us to fit well the nuclear magnetization curves $M(t)$ over the entire experimental temperature range and to obtain the T dependencies of T_1^{-1} in a single unified approach. Here M_0 is the equilibrium nuclear magnetization, b is the stretching parameter, and T_1 is the spin-lattice relaxation time. A typical example of the NMR echo intensity decay and the corresponding fit are shown in Fig. 16. The stretching parameter b is close to unity in the paramagnetic regime at high temperatures and reduces to smaller values in the spin-correlated regime, indicating a distribution of relaxation rates at lower temperatures.

In general, in magnetic materials the NMR T_1^{-1} relaxation rate reads

$$\frac{1}{T_1} = \frac{k_B T}{\hbar^2} \sum_q |A(\mathbf{q})|^2 \frac{\chi''(\mathbf{q}, \omega_L)}{\omega_L}. \tag{5}$$

Here the sum is over the wave vectors $\mathbf{q}$ within the first Brillouin zone, $A(\mathbf{q})$ is a form factor depending on the $\mathbf{q}$ vector, k_B is the Boltzmann constant, ω_L is the Larmor frequency, and χ'' is the imaginary part of the dynamic susceptibility. In the paramagnetic regime, Eq. (5) simplifies to

$$\frac{1}{T_1} \propto T\chi, \tag{6}$$

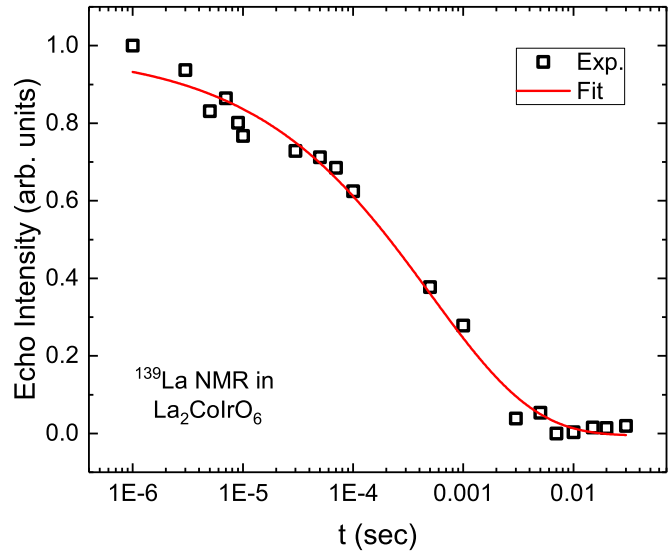

FIG. 16. Time evolution of the spin echo intensity of the ^{139}La nuclei measured at the maximum of the NMR line intensity. Solid line is the fit according to Eq. (4).

where χ is the uniform static electron spin susceptibility. Filtering effects, such as that the hyperfine coupling is peaked (or zero) for certain $\mathbf{q}$ vectors, are expected to be small for the studied materials since the La sites are coupled to several transition metal sites implying a weak dependence of A on $\mathbf{q}$.

In Fig. 17(a) the T dependence of the spin-lattice relaxation rate $T_1^{-1}(T)$ for La_2ZnIrO_6 is presented. At high temperatures it is almost constant and after a slight increase around $T \approx 30$ K, $T_1^{-1}(T)$ rapidly decreases by further lowering the temperature. A sharp peak in $T_1^{-1}(T)$ is observed at $T \approx 11$ K, with experimental resolution of better than 1 K, which corresponds to the magnetic phase transition in La_2ZnIrO_6.

In contrast to La_2ZnIrO_6, the peak at the ordering temperature in the T dependence of the $T_1^{-1}(T)$ for La_2CoIrO_6 is much broader [Fig. 18(a)]: the relaxation rate continuously increases from room temperature down to $T_N = 98$ K where it reaches a maximum followed by a rapid slowing down at $T < T_N$. The nuclear spin-lattice relaxation rate T_1^{-1} in an antiferromagnetically ordered state is mainly driven by scattering of nuclear spins off magnons, that usually leads to a power-law temperature dependence [32]. When the temperature energy scale $k_B T$ is larger than the magnon gap, T_1^{-1} follows a T^3 or T^5 dependence for the two- and three-magnon Raman processes, respectively. As can be seen in Fig. 18(a), the ^{139}La nuclear relaxation rate in La_2CoIrO_6 at $T < T_N$ can be at best described as $T_1^{-1} \propto T^3$, suggesting that it is dominated by the two magnon Raman process, which is, indeed, expected for canted antiferromagnets [32].

The relaxation rate T_1^{-1} in La_2CoIrO_6, as well as in La_2CuIrO_6 [17], is much smaller than that in La_2ZnIrO_6. At first glance this is surprising, since according to Eq. (5), $T_1^{-1} \propto A_{hp}^2$, and thus in the case of the first two compounds the fluctuating hyperfine fields from both $3d$ and $5d$ electron spins should contribute to the nuclear-spin relaxation as $T_1^{-1} \propto (A_{hp,Co/Cu}^2 + A_{hp,Ir}^2)$, making it faster than in the third compound. However, one has to keep in mind that the relax-

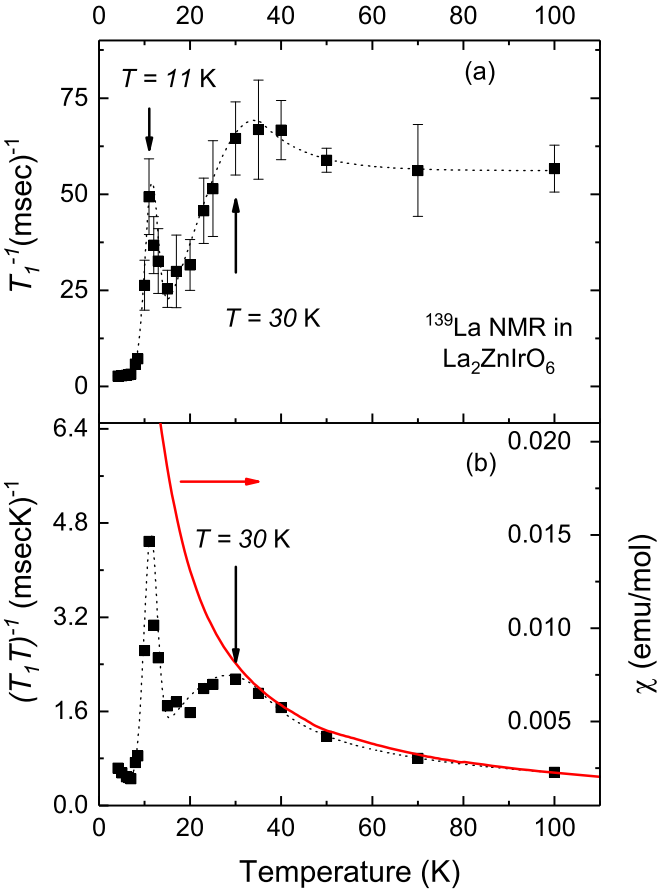

FIG. 17. (a) Temperature dependence of the ^{139}La T_1^{-1} relaxation rate for La_2ZnIrO_6. Dotted line is a guide for the eye. (b) T dependence of the dynamic susceptibility $(T_1T)^{-1}$ for La_2ZnIrO_6. Dotted line is a guide for the eye. Red solid curve corresponding to the right axis is the bulk static susceptibility χ measured at a field 7 T.

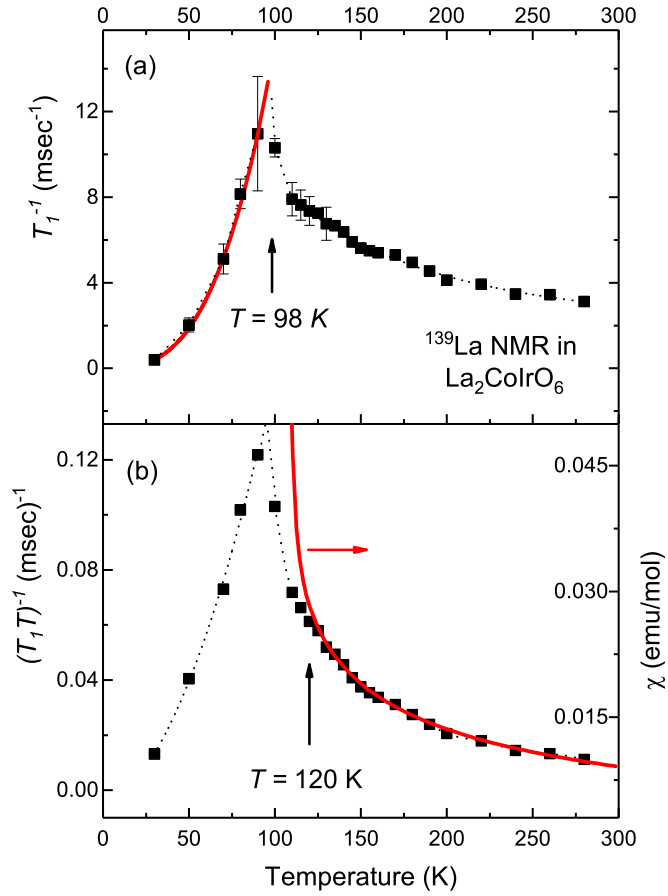

FIG. 18. (a) Temperature dependence of the ^{139}La T_1^{-1} relaxation rate for La_2CoIrO_6. Black dotted line is to guide the eye. Red solid line is a fit according to the two-magnon Raman process (see the text). (b) T dependence of the dynamic susceptibility $(T_1T)^{-1}$. Black dotted line is to guide the eye. Red solid curve corresponding to the right axis is the bulk static susceptibility χ measured at a field of 7 T.

ation process may become more effective if the frequency of electron spin fluctuations gets closer to the Larmor frequency ω_L of the nuclei under investigation. Hence, the observed hierarchy of the relaxation rates $T_{1,\mathrm{Zn}}^{-1} > T_{1,\mathrm{Cu}}^{-1} > T_{1,\mathrm{Co}}^{-1}$ suggests an increase of the frequency scale of the dynamics of the electron spin system in La_2BIrO_6 on the way from the nonmagnetic $3d$ subsystem in the case of $B = \mathrm{Zn}$ ($3d^{10}$, $S = 0$), to the "moderately" magnetic $B = \mathrm{Cu}$ ($3d^9$, $S = 1/2$), and to the strongly magnetic $B = \mathrm{Co}$ ($3d^7$, $S = 3/2$) $3d$ subsystems. This effect is likely to be related to the strong exchange coupling of the $3d$ spins and $5d$ $j_{\mathrm{eff}} = 1/2$ pseudospins in La_2CuIrO_6 and La_2CoIrO_6, as seen in the ESR experiments, which may reduce the low-frequency contribution to the electron spin fluctuation spectrum.

IV. DISCUSSION

In La_2ZnIrO_6 the ESR signal becomes first visible at $T \lesssim 30$ K. Interestingly, the broad maximum of the dynamic electron spin susceptibility measured by the NMR spin-lattice relaxation $\chi'' \propto (T_1T)^{-1}$ is also located at this temperature and χ'' begins to deviate from the static susceptibility towards the smaller values [Fig. 17(b)]. The latter is unusual since typically the local dynamic spin susceptibility probed by NMR is enhanced due to the slowing down of the electron spin fluctuations. The observed behavior can be explained by a partial compensation of the local field of surrounding electron spins at the given ^{139}La site due to strong AFM correlations. Besides, in the same temperature range the NMR line acquires a rectangular-like shape typical for AFM-ordered compounds (Fig. 11). All these observations point to a gradual establishment of the short-range AFM order in this temperature regime. At T_N amounting to ≈11 K at 7 T the long-range canted AFM order sets in. This is manifested in a sharp peak of the relaxation rate $T^{-1}(T)$ [Fig. 17(a)], a substantial line shift, a change of the lineshape (Fig. 11), and opening of the gap for the ESR excitation (Fig. 6).

In La_2CoIrO_6, the ESR mode emerges at $T \lesssim 140$ K (Fig. 8). Although, there is no broad maximum of $(T_1T)^{-1}$ as it was the case for La_2ZnIrO_6, the nuclear spin-lattice relaxation begins to grow significantly already at $T \sim 200$ K, providing evidence of strong electron-spin correlations [Fig. 18(a)]. Similar to La_2ZnIrO_6, the dynamic spin susceptibility $\chi'' \propto (T_1T)^{-1}$ deviates towards smaller values as compared with the static one [Fig. 18(b)]. This deviation

takes place at ∼120 K where also the NMR lineshape strongly changes (Fig. 10). This temperature is comparable with the temperature where the ESR mode appears. The phase transition to a canted AFM-ordered state takes place at $T_N = 98$ K at 7 T. It is accompanied by a sharp peak of the NMR relaxation rate $T_1^{-1}(T)$, a rectangular-like shape of the NMR line, and opening of the gap for the ESR mode.

The double perovskite structure is composed of two interpenetrating simple perovskite sublattices. In the case of La_2ZnIrO_6, only one of them is magnetic. As discussed above, this subsystem is characterized by a pronounced short-range-ordered regime above T_N. In contrast, La_2CoIrO_6 consists of two magnetic subsystems. The Co subsystem with the large spin $S = 3/2$ is dominating over the weaker magnetic subsystem of Ir pseudospins $j_{\text{eff}} = 1/2$. However, the magnetic behavior of the La_2CoIrO_6 compound above T_N appears unexpectedly similar to La_2ZnIrO_6: with the substantially higher ordering temperature T_N it demonstrates an extended temperature regime of strong AFM correlations characterized by a continuous slowing down of electron spin dynamics. The situation changes radically, if the two subsystems of the double perovskite are equivalent in terms of the spin value as it is the case in La_2CuIrO_6 with Cu^{2+} ($S = 1/2$) and Ir^{4+} ($j_{\text{eff}} = 1/2$). As our NMR data in Ref. [17] show, there is no such extended regime of strong correlations above T_N in this compound. Such correlations are visible there only on the very short picosecond timescale, as revealed by ESR [17].

The short-range ordered regime extended well above the ordering temperature T_N, observed in our experiments, indicates frustration of magnetic interactions in La_2CoIrO_6 and La_2ZnIrO_6 which tend to suppress the long-range order. It is known that the double perovskite lattice is inherently geometrically frustrated as it is composed of two intersecting fcc sublattices. The strong spin-orbit coupling yields a strongly anisotropic distribution of the spin density of the Ir ion which further enhances frustration [7]. In addition, the frustration is also likely to be related to the occurrence of the multiple exchange paths characteristic of the double perovskites which could be particularly boosted in the case of the spatially extended 5*d* orbitals (see, e.g., Refs. [8–10]). Finally, the t_{2g} orbitals of the Co^{2+} ions carrying an orbital moment are involved in the exchange paths which brings an additional complexity in the system. On the other hand, in La_2CuIrO_6 the Cu^{2+} ions with the active e_g orbitals carry no orbital momentum and have spin $S = 1/2$. It appears that the magnetic lattice in La_2CuIrO_6 composed of two "equally magnetic" subsystems is much less frustrated, possibly mostly due to the reduction of the geometrical frustration.

In both "two-component" systems, La_2CoIrO_6 and La_2CuIrO_6, at $T < T_N$ there is a gradual development of the coupling between the magnetic 3*d* and 5*d* subsystems. This is, reflected in a gradual evolution of the ESR response and in a continuous slowing down of the spin dynamics below T_N probed by the NMR relaxation. It seems that at T_N only the Co-spin sublattice in La_2CoIrO_6 orders, whereas the Ir-pseudospin sublattice is in the short-range correlated regime. The gradual evolution of the ESR signal below T_N provides evidence that, indeed, the magnetic system of exchange-coupled Co- and Ir-sublattices remains "soft" down to temperatures of the order ∼30 K where presumably the Ir-pseudospin sublattice orders long range. This scenario is supported by the evolution of the NMR spectrum whose shape acquires a typical AFM-like rectangular form (smoothed due to the quadrupolar splitting) only below 50 K (Fig. 12). We admit that the ordering of the Ir-spin sublattice in La_2CoIrO_6 still remains an open issue since, unfortunately, neutron diffraction experiments performed in Ref. [18] could determine the spin-ordered structure of the Co-subsystem only and could not provide any information regarding the spin order of the Ir-subsystem. The situation is somewhat different in La_2CuIrO_6 composed of two magnetic sublattices of a similar strength which may reduce geometrical frustration. Feasibly for this reason the cross coupling between the two subsystems develops in a significantly smaller temperature range and both Cu and Ir sublattices are involved in the ordering process at 74 K [17]. The remaining frustration due to the orbital degrees of freedom of Ir ions maintains the residual spin dynamics down to 54 K. In contrast, in the "one-component" La_2ZnIrO_6 the magnetic frustration is released below T_N. Therefore, the electron spin fluctuations in the ordered state decrease very sharply as evidenced by the NMR relaxation (Fig. 17).

V. CONCLUSIONS

In summary, we have studied with ESR and ^{139}La NMR spectroscopic techniques the static and dynamic magnetic properties of the two Ir-based double perovskites La_2CoIrO_6 and La_2ZnIrO_6. Both methods reveal pronounced quasistatic electron spin correlations at temperatures far above the magnetic phase transition at $T_N \approx 98$ and 11 K, respectively, signifying substantial frustration of exchange interactions. In La_2ZnIrO_6, comprising only one magnetic sublattice, the spin fluctuations freeze very rapidly below T_N, whereas in the "two-component" Co-Ir double perovskite magnetic lattice in La_2CoIrO_6, the spin dynamics decays continuously down to low temperatures. In particular, the NMR relaxation reveals substantial spin excitations over an extended temperature range below T_N, while in the La_2ZnIrO_6 compound the magnon gap of the order of $k_B T_N$ obviously suppresses the magnon dynamics. Moreover, the analysis of the negative hyperfine coupling of the ^{139}La nuclei to the Ir 5*d* moments indicates that the La 4*d* orbitals are involved in the exchange interaction between the Ir 5*d* moments, whereas the positive coupling of the ^{139}La nuclei to the 3*d* Cu or Co orbital is simply a transferred one which does not involve the La 4*d* orbitals. The obtained results point at the important role of the multiple, competing exchange pathways involving spatially extended, strongly anisotropic 5*d* magnetic orbitals in the Ir-based double perovskites and call for further development of theoretical concepts behind the nontrivial magnetism of this type of strongly spin-orbit coupled materials.

ACKNOWLEDGMENT

This work was supported by the Deutsche Forschungsgemeinschaft (DFG) through Grant No. KA 1694/8-1, SFB 1143 (Project B01) and the Emmy Noether Grant No. WU 595/3-3.

[1] G. Cao and L. E. DeLong, *Frontiers of 4d- and 5d-Transition Metal Oxides* (World Scientific, Singapore, 2013).

[2] W. Witczak-Krempa, G. Chen, Y. B. Kim, and L. Balents, Annu. Rev. Condens. Matter Phys. **5**, 57 (2014).

[3] J. G. Rau, E. K.-H. Lee, and H.-Y. Kee, Annu. Rev. Condens. Matter Phys. **7**, 195 (2016).

[4] S. M. Winter, A. A. Tsirlin, M. Daghofer, J. van den Brink, Y. Singh, P. Gegenwart, and R. Valentí, J. Phys.: Condens. Matter **29**, 493002 (2017).

[5] G. Cao and P. Schlottmann, Rep. Prog. Phys. **81**, 042502 (2018).

[6] K. V. Shanavas, Z. S. Popović, and S. Satpathy, Phys. Rev. B **90**, 165108 (2014).

[7] G. Jackeli and G. Khaliullin, Phys. Rev. Lett. **102**, 017205 (2009).

[8] R. Morrow, R. Mishra, O. D. Restrepo, M. R. Ball, W. Windl, S. Wurmehl, U. Stockert, B. Büchner, and P. M. Woodward, J. Am. Chem. Soc. **135**, 18824 (2013).

[9] X. Ou, Z. Li, F. Fan, H. Wang, and H. Wu, Sci. Rep. **4**, 7542 (2014).

[10] S. Kanungo, B. Yan, C. Felser, and M. Jansen, Phys. Rev. B **93**, 161116 (2016).

[11] G. Cao, A. Subedi, S. Calder, J.-Q. Yan, J. Yi, Z. Gai, L. Poudel, D. J. Singh, M. D. Lumsden, A. D. Christianson, B. C. Sales, and D. Mandrus, Phys. Rev. B **87**, 155136 (2013).

[12] A. A. Aczel, A. M. Cook, T. J. Williams, S. Calder, A. D. Christianson, G.-X. Cao, D. Mandrus, Y.-B. Kim, and A. Paramekanti, Phys. Rev. B **93**, 214426 (2016).

[13] W. K. Zhu, C.-K. Lu, W. Tong, J. M. Wang, H. D. Zhou, and S. X. Zhang, Phys. Rev. B **91**, 144408 (2015).

[14] G. Demazeau, B. Siberchicot, S. Matar, C. Gayet, and A. Largeteau, J. Appl. Phys. **75**, 4617 (1994).

[15] M. Uhl, S. F. Matar, and B. Siberchicot, J. Magn. Magn. Mater. **187**, 201 (1998).

[16] R. C. Currie, J. F. Vente, E. Frikkee, and D. Ijdo, J. Solid State Chem. **116**, 199 (1995).

[17] K. Manna, R. Sarkar, S. Fuchs, Y. A. Onykiienko, A. K. Bera, G. A. Cansever, S. Kamusella, A. Maljuk, C. G. F. Blum, L. T. Corredor, A. U. B. Wolter, S. M. Yusuf, M. Frontzek, L. Keller, M. Iakovleva, E. Vavilova, H.-J. Grafe, V. Kataev, H.-H. Klauss, D. S. Inosov, S. Wurmehl, and B. Büchner, Phys. Rev. B **94**, 144437 (2016).

[18] N. Narayanan, D. Mikhailova, A. Senyshyn, D. M. Trots, R. Laskowski, P. Blaha, K. Schwarz, H. Fuess, and H. Ehrenberg, Phys. Rev. B **82**, 024403 (2010).

[19] A. Kolchinskaya, P. Komissinskiy, M. B. Yazdi, M. Vafaee, D. Mikhailova, N. Narayanan, H. Ehrenberg, F. Wilhelm, A. Rogalev, and L. Alff, Phys. Rev. B **85**, 224422 (2012).

[20] M. Vogl, L. T. Corredor, T. Dey, R. Morrow, F. Scaravaggi, A. U. B. Wolter, S. Aswartham, S. Wurmehl, and B. Büchner, Phys. Rev. B **97**, 035155 (2018).

[21] C. Golze, A. Alfonsov, R. Klingeler, B. Büchner, V. Kataev, C. Mennerich, H.-H. Klauss, M. Goiran, J.-M. Broto, H. Rakoto, S. Demeshko, G. Leibeling, and F. Meyer, Phys. Rev. B **73**, 224403 (2006).

[22] C. P. Poole, *Electron Spin Resonance: A Comprehensive Treatise on Experimental Techniques* (Dover Publications, Mineola, New York, 1996).

[23] A. Abragam and B. Bleaney, *Electron Paramagnetic Resonance of Transition Ions*, International Series of Monographs on Physics (Oxford University Press, Oxford, 2012).

[24] N. A. Bogdanov, V. M. Katukuri, J. Romhanyi, V. Yushankhai, V. Kataev, B. Buechner, J. van den Brink, and L. Hozoi, Nat. Commun. **6**, 7306 (2015).

[25] P. Battle and J. Gore, J. Mater. Chem. **6**, 1375 (1996).

[26] E. A. Turov, in *Physical Properties of Magnetically Ordered Crystals*, edited by A. Tybulewicz and S. Chomet (Academic Press, New York, 1965).

[27] H. J. Fink and D. Shaltiel, Phys. Rev. **130**, 627 (1963).

[28] S. J. Williamson and S. Foner, Phys. Rev. **136**, A1102 (1964).

[29] J. O. Artman, Phys. Rev. **105**, 74 (1957).

[30] N. Vukadinovic, J. Youssef, and H. L. Gall, J. Magn. Magn. Mater. **150**, 213 (1995).

[31] A. Abragam, *Principles of Nuclear Magnetism* (Clarendon Press, Oxford, 1961).

[32] D. Beeman and P. Pincus, Phys. Rev. **166**, 359 (1968).